NMR-Paramagnetic Relaxation Due to the High-Spin d^3 Electron Configuration: Cr(III)−TSPP

Nathaniel Schaefle and Robert Sharp*

Department of Chemistry, The University of Michigan, Ann Arbor, Michigan 48109-1055

Received: October 26, 2004; In Final Form: February 5, 2005

Sulfonated metalloporphyrins (Me−TSPP, where Me = Cr(III), Mn(III), Fe(III), and Mn(II)) comprise a well-characterized series of water-soluble paramagnetic complexes with electron spins of $S = {}^3/_2$, 2, ${}^5/_2$, and ${}^5/_2$, respectively, which provide important model systems for mechanistic studies of paramagnetic NMR relaxation in solution. Previous studies of Mn(III), Fe(III), and Mn(II)−TSPP have uncovered relaxation mechanisms which differ qualitatively from each other and exhibit numerous unexpected features. In this study, Cr(III)−TSPP was examined as a model system for the d^3 $S = {}^3/_2$ electron configuration. Magnetic relaxation dispersion (MRD) profiles of the water proton R_1 were measured as a function of pH between pH 1 and pH 9. In acid samples, R_1 results from acid-catalyzed prototropic chemical exchange involving the Cr(III)−TSPP·$2H_2O$. In neutral and basic solution, this species deprotonates, and base-catalyzed prototropic exchange becomes important. The pH 1 data were analyzed quantitatively using theory that accounts for the role of the permanent zero field splitting (zfs) tensor and for the effects of Brownian reorientation. Two levels of theory were employed: (1) spin dynamics simulation, which accurately describes the effects of Brownian reorientation on the spin wave functions, and (2) the "constant H_S" approximation, which incorporates the effects of multiexponential electron spin relaxation and facilitates the physical interpretation of the relaxation mechanism. It was found that neither level of theory alone provides a fully satisfactory quantitative description of the data due to the fact that both reorientational modulation of the spin wave functions and multiexponential electron spin relaxation are important. The zero field splitting parameter, $D = 0.27$ cm^{-1}, is well defined by the data and was measured.

Introduction

The metalloporphyrins (Me−TSPP, where Me = Cr(III), Mn(III), Fe(III), and Mn(II)), shown in Figure 1, comprise a well-characterized series of water-soluble paramagnetic complexes with electron spins of $S = {}^3/_2$, 2, ${}^5/_2$, and ${}^5/_2$, respectively (all are high-spin in aqueous solution). They are particularly important model systems for mechanistic studies of paramagnetic NMR relaxation because of physical and chemical constraints imposed by the 4-fold rotational symmetry of the complex. In this environment, the form of the zero field splitting (zfs) tensor is simple and well defined: the unique zfs tensor axis coincides with the rotation axis, and the orthorhombic zfs tensor components vanish; only the axial components of the zfs tensor (D and B_4^0), plus, for $S \geq 2$, a tetragonal fourth-order component, B_4^4, are nonzero. Chemically, Me−TSPP complexes are relatively well defined and well characterized with respect to the important physical parameters of the NMR relaxation mechanism.

Previous work from our laboratory has characterized the relaxation mechanisms operating in TSPP complexes of Mn(II)[1] (using data reported by Bryant et al.[2]), Mn(III),[3,4] and Fe(III).[5] The mechanisms of these three spin systems differed qualitatively from each other and exhibited numerous unexpected features. For Mn(III)−TSPP ($S = 2$), the magnetic relaxation dispersion (MRD) profiles (i.e., the profiles of the water proton R_1 relaxation rate as a function of laboratory field strength) are determined principally by a small splitting in the $m_S = \pm 2$ non-Kramers doublet that is induced by the tetragonal fourth-order component, B_4^4, of the zfs tensor. The axial quadratic zfs term, D, while an order of magnitude larger than B_4^4, has little influence on the shape or magnitude of the MRD profile. For Fe(III)−TSPP ($S = {}^5/_2$ with a large zfs interaction), the shape of the MRD profile is likewise controlled by the tetragonal fourth-order zfs component, although for this Kramers spin system, the role of the B_4^4 term in the relaxation mechanism is entirely different than that for $S = 2$, involving B_4^4-induced wave function mixing rather than, as for $S = 2$, breaking the degeneracy of the non-Kramers doublets. For Fe(III)−TSPP, the primary determinant of the shape of the MRD profile is the ratio B_4^4/D. Finally, for Mn(II)−TSPP ($S = {}^5/_2$, with a small zfs interaction), the form of the MRD profile is determined principally by the magnitude of the quadratic axial zfs term, D.

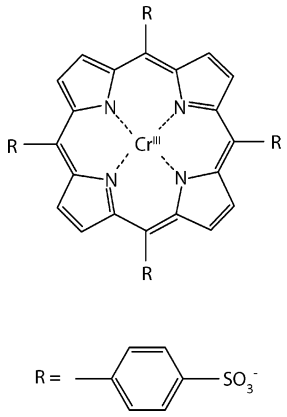

Figure 1. Structure of chromium(III) *meso*-tetra(4-sulfonatophenyl)-porphin (Cr(III)−TSPP).

10.1021/jp045115u CCC: $30.25
Published on Web 03/18/2005

We report here an experimental and theoretical study of the NMR relaxation mechanism for Cr(III)−TSPP ($S = {}^3/_2$). For this system, the zfs tensor contains only a quadratic axial component, D, the magnitude of which has not been measured previously but is expected to be the order of a few tenths of a wavenumber. We show below in theoretical simulations that the axial zfs tensor component produces a distinctive dispersive feature in the MRD profile, which defines the value of this parameter. This dispersive feature, which is present in the experimental profile, arises physically from the change of spatial quantization of the electron spin motion that occurs when, with increasing laboratory field strength, the electron spin Hamiltonian passes between the zfs and Zeeman limits. (The zfs and Zeeman limits are the regimes of laboratory field strength where the zfs energy is either large or small compared to the Zeeman energy. The zfs limit requires, additionally, that reorientation not be so fast that the zfs level structure is collapsed.) The principal unknowns in the analysis are the zfs D parameter and the electron spin relaxation times of the $m_S = \pm{}^1/_2$ and $\pm{}^3/_2$ Kramers doublets.

Theoretical MRD profiles for $S = {}^3/_2$, calculated at different levels of theory and different physical assumptions, have been published by Westlund et al.,[6] Bertini et al.,[7,8] Kruk et al.,[9] Nilsson and Kowalewski,[10,11] and Sharp.[12] Prior experimental MRD work for Cr(III) is not very extensive. In a recent Cr(III) study, Miller et al.[13] analyzed the MRD data of Wang et al.[14] for the methyl ^{1}H resonance of Cr(III)(acac)$_3$ dissolved in $CHCl_3$. This complex is very well defined both structurally and with respect to its zfs properties; in fact, all of the important parameters of theory are known (or, at least, fairly tightly constrained) by data from other experiments, so that a direct calculation of the MRD profile (as opposed to a fit involving the variation of undetermined parameters) should be possible. However, a theoretical analysis using spin dynamics (SD) methods that are believed to describe the principal aspects of the NMR relaxation mechanism was not entirely successful. A quantitative simulation of the data was achieved only by assuming an orientation of the electron-nuclear interspin vector that appeared inconsistent with the molecular structure. The difficulty of achieving a straightforward calculation of the MRD profile in this very well-defined system is puzzling.

The form of the MRD profile depends in an intimate way on the electron spin level diagram. There is a strong dependence on the electron spin quantum number as well as on the electron configuration; for example, $S = {}^3/_2$ arising from a d^3 configuration (Cr(III)) has very different spin properties than $S = {}^3/_2$ arising from a d^7 configuration (high-spin Co(II)). Our long-term objective is to understand this relationship quantitatively for different electron spin systems. The present study examines Cr(III)−TSPP as a model for the high-spin d^3 spin system.

Experimental Section

Chromium(III) *meso*-tetra(4-sulfonatophenyl)porphine chloride (Cr(III)−TSPP) was purchased from Frontier Scientific (Logan, Utah). Aqueous buffered samples were prepared with Cr(III)−TSPP concentrations between 1.0 and 1.2 mM porphyrin in a series of buffers at pH 1−9 with total buffer concentrations of 50.0 mM. Hydrion dry buffer salts from Aldrich were used for samples at pH 2−9 (buffer composition: pH 2 and 3 were biphthalate/sulfamic acid, pH 4 was biphthalate, pH 5, 6, 7, and 8 were phosphate, and pH 9 was carbonate). The pH 1 buffer was the certified HCl/NaCl standard from Fisher Scientific. The samples were placed in 7 mm, acid-washed borosilicate test tubes, degassed by a series of five freeze−pump−thaw cycles, and sealed under vacuum. Distilled, deionized water was taken from a Barnsted Millipore filtration system with both ionic and organic sections that used deionized water as the feed. UV−visible absorption spectra were collected on a Shimadzu UV1601 spectrometer.

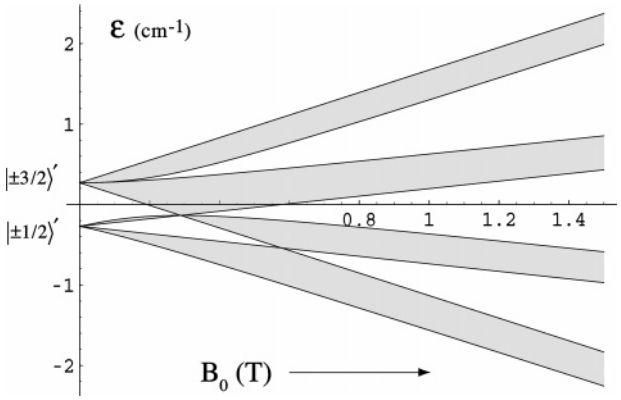

Figure 2. Energy band structure for $S = {}^3/_2$ assuming $D = 0.27$ cm^{-1} and $E = 0$.

NMR T_1 relaxation times were measured at frequencies of 0.6−70 MHz at 20 °C using a tunable NMR spectrometer.[15] Spin−lattice relaxation times were measured using the phase shifted triplet sequence,[16] $(\pi)_\pi - [\tau_d - (\pi/2)_0 - \tau_{tr} - (\pi)_\pi - \tau_{tr} - (\pi/2)_0]_n$, in which the magnetization is sampled by pulse triplets at successive intervals, τ_d, during the decay. The reproducibility of this method on a given sample is ±1.0% when $(\tau_{tr}/\tau_d) \leq 0.01$. At low field strengths, the signal-to-noise ratio was relatively poor and averaging was used to obtain a reproducibility of 3% or better. The sample probe temperature was maintained within ±0.5 °C via a stream of dry nitrogen.

Theory

For $S = {}^3/_2$, the electron spin Hamiltonian, including Zeeman and zfs interactions, can be written as

$$H_S(\beta,\gamma;t) = H_{Zeem} + H^{\circ}_{zfs}(\beta,\gamma;t) \tag{1a}$$

$$= g_e\beta_e\vec{B}_0\cdot\vec{S} + D(\hat{S}_z^{\,2} + S(S+1)/3) + E(\hat{S}_x^{\,2} - \hat{S}_y^{\,2}) \tag{1b}$$

The Hamiltonian, $H^{\circ}_{zfs}(\beta,\gamma;t)$, of the permanent zfs interaction depends on the polar angles, β and γ, specifying the orientation of the laboratory magnetic field in the zfs principal axis system (PAS). The spin operators in the second and third terms of eq 1b are defined relative to the zfs PAS, as denoted by a circumflex ($\wedge$) on the spin operators. In the D_{4h} site symmetry of Cr(III)−TSPP, the orthorhombic zfs term, E, vanishes. The quantities g_e, β_e, and B_0 are the electron g value, the Bohr magneton, and the laboratory field strength. For Cr(III), $g_e = 1.99$ was assumed.[17] The D parameter has not been measured for Cr(III)−TSPP. ESR studies of six-coordinate complexes with tetragonal[18,19] and trigonal[20] fields have given values in the range 0.03−2 cm^{-1}.

The electron spin level diagram and spin eigenfunctions for $S = {}^3/_2$ are shown in Figure 2. The level diagram depends on the polar angle, β, between $\vec{B}_0$ and $\hat{z}$. For powders, the spread of energy levels when both a permanent zfs interaction and a Zeeman field are present is shown in the figure. The range of B_0 corresponds approximately to the experimental range of MRD data shown below. In the zfs limit, the energy levels form two Kramers doublets, $m_S = \pm{}^1/_2$ and $\pm{}^3/_2$, separated by $2D$. With increasing B_0, the levels split and broaden into bands. In

the Zeeman limit, there are four bands, each of width $2D$, corresponding to the $+^3/_2$, $+^1/_2$, $-^1/_2$, and $-^3/_2$ eigenstates of the Zeeman-only spin Hamiltonian.

In the cylindrical zfs limit (small B_0), the spin eigenfunctions can be taken as the circularly polarized functions, $|\pm^1/_2\rangle'$ and $|\pm^3/_2\rangle'$, spatially quantized along $\hat{z}$. The energy levels form two Kramers doublets, $m_S = \pm^1/_2$ and $\pm^3/_2$, separated by $2D$. With increasing B_0, the levels broaden into bands, and the spin wave functions become complex admixtures of the zfs-limit basis functions. In the intermediate regime, the spin eigenfunctions lack well-defined spatial polarization. At high laboratory field strength (the vicinity of Zeeman limit), the spin eigenfunctions approach the circularly polarized Zeeman basis functions, $|\pm^1/_2\rangle$ and $|\pm^3/_2\rangle$, spatially quantized along $\vec{B}_0$. Even at high field strengths, however, the permanent zfs interaction mixes Zeeman basis functions with $\Delta m_S = \pm 1$ and ± 2, leading to the band structure in the high-field region of Figure 2.

NMR-Paramagnetic Relaxation Enhancement (NMRPRE). The water proton R_1 relaxation rate consists of inner and outer sphere contributions. The former results from Cr(III)-bound water protons which are in rapid chemical exchange equilibrium with unbound water molecules in the bulk solvent. This contribution is described by the Luz−Meiboom equation[21]

$$R_{1p} = \frac{f_M}{T_{1M} + \tau_M} \tag{2}$$

where f_M is the mole fraction of exchangeable water protons that are present in the metal coordination sphere, T_{1M}^{-1} is the spin−lattice relaxation rate of bound protons, and τ_M is the chemical exchange residence time of protons in the bound site. The Cr(III) ion is exchange-inert, and thus, proton chemical exchange is assumed to be prototropic. (The first-order chemical exchange rate constant for water molecules on $Cr(H_2O)_6^{3+}$ is 4×10^{-4} s^{-1} at 25 °C.[22,23] The anation reactions of Cr(III)−TSPP$\cdot(H_2O)_2^{3-}$, while faster, occur on a time scale of hundreds of seconds.[24−26]) Prototropic chemical exchange of water protons in metal complexes is usually thought to be acid- or base-catalyzed.[27] Defining q as the number of exchangeable protons per Cr(III) gives $f_M = q$[Cr(III)]/111.

Calculation of T_{1M}. For water protons, T_{1M} is principally determined by the electron-nuclear magnetic dipole−dipole interaction. The Zeeman-limit (SBM) theory is well-known.[28−30] More general formulations of the problem which are capable of incorporating a spin Hamiltonian of the form of eqs 1a and b have been described.[31] Calculations of the NMR-PRE can be performed at various levels of approximation, all of which involve significant assumptions. Work in our laboratory uses two basic approaches, namely, spin dynamics (SD) simulation and "constant H_S" theory, and they are implemented in the computer program Parelax2. Reference 32 contains a systematic description of the theory. In Florence, Bertini et al.[8] have developed a program which implements constant H_S algorithms similar to those employed in our earlier program called Parelax.[33] In Sweden, Kowalewski, Westlund, and their co-workers[34,35] have developed a formalism based on the stochastic Liouville equation (SLE) that provides a similar level of description to SD simulation.

Spin Dynamics Simulation. NMR-PRE depends on the Fourier−Laplace transform of the time-correlation function (TCF), $\{\langle H_{IS}(t)\, H_{IS}(0)\rangle\}_{ea}$, of the electron-nuclear dipole−dipole Hamiltonian. The broken brackets denote a trace over spin variables, and the braces denote an ensemble average over molecular degrees of freedom. SD methods simulate this TCF directly in the time domain.[1,4,13,36] The motion of the spin operators is propagated quantum mechanically, and molecular reorientation is modeled classically using a random walk model based on the work of Ivanov.[37] The calculation is difficult when ($H^\circ_{zfs} \geq H_{Zeem}$), since the spin eigenfunctions and eigenfrequencies are stochastic functions of time, and the interspin vector, $\vec{r}_{IS}$, and the spin Hamiltonian, $H_S(\beta,\gamma;t)$, undergo correlated motions. SD simulates these phenomena in a straightforward and accurate way.

Constant H_S Approximation. A deficiency of SD is that time-domain simulations do not readily incorporate level-specific electron spin relaxation (i.e., for $S = ^3/_2$, electron spin relaxation times which differ in the $m_S = \pm^1/_2$ and $\pm^3/_2$ Kramers doublets). Also, SD simulations lack physical transparency in terms of the contributions of specific eigenstates, spin matrix elements, and so forth. These deficiencies are remedied in part in the constant H_S approximation, which treats the electron spin Hamiltonian as in a powder; the reorientational time dependence of $H^\circ_{zfs}(\alpha,\beta;t)$ in eq 1a is neglected, and $H_S(\beta,\gamma;t)$ can be written as $H_S(\beta,\gamma)$. Although the effect of Brownian reorientation on $H_S(\beta,\gamma;t)$ is neglected, the stochastic motions of $\vec{r}_{IS}(t)$, which damp the dipole−dipole TCF, are retained in the form of a damping factor, $\exp(-t/\tau_R)$.

In the constant H_S algorithms of Parelax2, $H_S(\beta,\gamma)$ is diagonalized at a sequence of discrete molecular orientations, at each of which the NMR relaxation rate, R_{1M}, is calculated as a sum of contributions due to spin matrix elements, $\langle\mu|\hat{S}_p^{(1)}|\nu\rangle$, evaluated in the eigenbasis of $H_S(\beta,\gamma)$. These contributions are averaged spatially using a model in which (β,γ) are defined by the set of 92 orientations corresponding to the vertices and face centers of the truncated icosahedron (buckeyball). In the constant H_S expressions, the contributions to R_{1M} of specific spin matrix elements are isolated in a way that is not possible in the time-domain simulations of SD because in SD the eigenbasis is time-dependent. The constant H_S formulation also incorporates multiexponential electron spin relaxation times, which SD does not. Neither SD simulation nor constant H_S provides an entirely satisfactory description; the former provides a more realistic description of the effects of Brownian motion, and the latter provides a transparent physical picture and is able to incorporate multiexponential electron spin relaxation times. We use the two methods in parallel to provide as full a picture of the relaxation mechanism as possible.

The molecular-frame (MF) constant H_S expression for T_{1M} is[32]

$$\begin{aligned} R_{1M} = -48\pi(\gamma_I g_e \beta_e)^2 r_{IS}^{-6} (\mu_0/4\pi)^2 \sum_{q,q'=-1}^{1} \sum_{p,p'=-1}^{1} \\ \times \begin{bmatrix} 1 & 2 & 1 \\ p & (q-p) & -q \end{bmatrix} \begin{bmatrix} 1 & 2 & 1 \\ p' & (-q'-p') & q' \end{bmatrix} \\ \times (-1)^{q+q'} Y_{2,q-p}(\hat{\theta},\hat{\varphi})\, Y_{2,q'-p'}(\hat{\theta},\hat{\varphi}) \\ \times \{ \mathscr{D}^{(1)}_{q,+1}(\alpha,\beta,\gamma)\, \mathscr{D}^{(1)}_{q',-1}(\alpha,\beta,\gamma) \\ \times (2S+1)^{-1} \sum_{\mu,\nu} \langle\mu|\hat{S}_p^{(1)}|\nu\rangle\langle\nu|\hat{S}_{p'}^{(1)}|\mu\rangle \hat{J}_p(\omega_{\mu\nu})\}_{ea} \end{aligned} \tag{3a}$$

$$\hat{J}_p(\omega_{\mu\nu}) = \frac{\hat{\tau}^{(\mu)}_{d,p}}{1 + (\omega_I - \omega_{\mu\nu})^2 (\hat{\tau}^{(\mu)}_{d,p})^2} \tag{3b}$$

where the quantities in square brackets are 3-j symbols, r_{IS} is the interspin distance, and μ_0 is the permeability of space. The

second-rank spherical harmonics, $Y_{2,q}(\hat{\theta},\hat{\varphi})$, have as arguments the polar angles of $\vec{r}_{IS}$ with respect to the zfs PAS. Circumflexes ($\wedge$) on spin and space variables denote a definition relative to the zfs PAS. The Wigner rotation matrix elements, $\mathscr{D}^{(1)}_{q,\pm 1-p}(\alpha, \beta, \gamma)$, rotate operators from the laboratory frame to the MF through the Euler angles, (α, β, γ). The spin matrix elements, $\langle\mu|\hat{S}^{(1)}_p|\nu\rangle$, are evaluated in the eigenbasis, $\{|\mu\rangle, |\nu\rangle\}$, of $H_S(\beta,\gamma)$; these quantities, and the eigenfrequencies, depend on the orientational variables, (β,γ). The braces denote an average over molecular orientations in the powder.

The dipolar correlation time in eq 3 is defined as

$$(\hat{\tau}^{(\mu)}_{d,r})^{-1} = (\tau_R)^{-1} + (\hat{\tau}^{(\mu)}_{S,r})^{-1} + (\tau_M)^{-1} \quad (4)$$

In the zfs limit, the reorientational correlation time, $\tau_R = \tau^{(1)}_R$ describes the motion of a first-rank, rather than a second-rank, molecule-fixed tensor, as is appropriate when the electron spin motion is quantized along molecule-fixed axes,[38] rather than along $\vec{B}_0$. In the Zeeman limit, $\tau_R = \tau^{(2)}_R$, as in SBM theory. The τ_R parameter in eq 4 contains an implicit magnetic field dependence in the intermediate regime, which is described accurately in SD simulation but not in constant H_S theory, which is not intended to provide an accurate description of the reorientational aspects of the problem.

Electron Spin Relaxation. The electron spin relaxation times, $\hat{\tau}^{(\mu)}_{S,r}$, in eq 4 in general depend on the eigenstate, μ, and the spatial polarization, $r = \hat{x},\hat{z}$.[39] For $S \geq 1$ metal ions, electron spin relaxation results from thermal modulation of the zfs tensor. When a permanent zfs interaction is present, this process involves both reorientation of the principal axes and collisional modulation of the tensor components. The reorientational zfs contribution is described quantitatively (including the magnetic field dependence) by an SD simulation using, as physical parameters, the permanent zfs coefficient, D, and $\tau^{(2)}_R$.

The Collisional zfs Mechanism. This mechanism was first considered by Bloembergen and Morgan[30] in a description of electron spin relaxation of aqueous transition metal cations. They derived the following Zeeman-limit ($H^\circ_{zfs} = 0$) expressions for $\tau_{S1,2}$:

$$(\tau_{S1})^{-1} = c_Z[j(\omega_S) + 4j(2\omega_S)] \quad (5a)$$

$$(\tau_{S2})^{-1} = c_Z[(^3/_2)j(0) + (^5/_2)j(\omega_S) + (2\omega_S)] \quad (5b)$$

where

$$c_Z = [4S(S+1) - 3](\Delta_t^2/5) \quad (5c)$$

$$j(\omega) = \tau_v/(1 + \omega^2\tau_v^2) \quad (5d)$$

where Δ_t is the mean-square amplitude of the transient zfs tensor associated with zfs distortion, ω_S is the electron Larmor frequency, and τ_v is the correlation time for zfs distortion. According to these expressions, $\tau_{S1,2}$ are field-independent in the field range where $\omega_S\tau_v < 1$, but they increase at higher field strengths due to the Zeeman splitting of the spin levels.

When a permanent zfs interaction is present, the energy band structure is broad and complex in the intermediate regime (Figure 2). The electron spin eigenfunctions, expressed in the eigenbasis of either H°_{zfs} or H_{Zeem}, are strong admixtures of the basis functions. Zfs-limit expressions analogous to eqs 5a−d have been derived for $S = 1$ by Westlund[40] and generalized to non-Redfield situations ($\tau_v \geq \tau_S$) by Bertini et al.[41] Sharp and Lohr[39] have derived Redfield expressions for arbitrary electron spin, which are valid for all field strengths, that is, for the zfs and Zeeman limits as well as for the intermediate regime ($H^\circ_{zfs} \approx H_{Zeem}$).

In the NMR experiment, electron spin relaxation occurs in a thermal equilibrium ensemble; that is, the electron spin density matrix remains at thermal equilibrium. In this situation, electron spin relaxation refers to the thermal decay of the TCFs of the electron spin components,[39] for example, TCFs such as $\langle S^{(1)}_x(t)\, S^{(1)}_x(0)\rangle$, rather than the decay of nonequilibrium parts of the density matrix. The decay constants for this process in general depend on spin eigenstate.[39] In the vicinity of the Zeeman limit, the decay modes are polarized spatially along laboratory axes (x,z), while, near the zfs limit, they are polarized along molecule-fixed axes ($\hat{x},\hat{y},\hat{z}$). In the intermediate regime, the spatial polarization is complex. Equations 3a and b are formulated in the MF, and the relevant spin relaxation times, $\hat{\tau}^{(\mu)}_{S,r}$, are likewise defined in the MF. In most cases, the physical information needed to calculate eigenstate-specific relaxation times is lacking, and it is appropriate then to employ the eigenstate-averaged quantities, $\hat{\tau}_{S,r}$, defined in ref 42:

$$(\hat{\tau}_{S,r})^{-1} = c_r\sum_q n^{(r)}_q\{\sum_{\mu,\nu}|\langle\mu|\hat{S}^{(2)}_q|\nu\rangle|^2\hat{j}(\omega_{\mu\nu}) + c.t.\}_{ea} \quad (6a)$$

$$c.t. = 3^{1/2}c_r\sum_{\mu,\nu}\langle\mu|\hat{S}^{(2)}_1|\nu\rangle\langle\nu|\hat{S}^{(2)}_2|\mu\rangle[2\hat{j}(\omega_{\mu\nu})] \quad (6b)$$

$$c_r = 3[S(S+1)(2S+1)]^{-1}(\Delta_t^2/5) \quad (6c)$$

$$\hat{j}(\omega_{\mu\nu}) = \tau_v/(1 + \omega_{\mu\nu}^2\tau_v^2). \quad (6d)$$

Equation 6 depends on the same two physical parameters, Δ_t^2 and τ_v, as appear in eq 5. The spin functions, $\hat{S}^{(2)}_q$, are second-rank Cartesian tensor functions of the spin operators (see the Appendix). The quantities, $n^{(r)}_q$, are integer coefficients which occur in double commutators of the spin operators (see the Appendix). The spin matrix elements and eigenfrequencies, $\omega_{\mu\nu}$, in eqs 6a and b are evaluated in the eigenbasis of $H_S(\beta,\gamma)$, and thus, they depend on molecular orientation. The braces in eq 6a represent an orientational average, which is carried out in Parelax2 using the "buckeyball" algorithm described above. The static zfs tensor coefficients, D and E, do not appear explicitly in these equations, but they are present implicitly in the form of $H_S(\beta,\gamma)$. The relaxation times, $\hat{\tau}_{S,r}$, in eq 6a are averaged with respect to both molecular orientation and spin eigenstate.

Results

General Features of the MRD Profiles. This section discusses the physical interpretation of the MRD profiles of Cr(III)−TSPP in terms of the theory of the previous section. Certain aspects of the NMR relaxation mechanism have not previously been described. The reader is also referred to the discussions in refs 6−12.

Figures 3 and 4 show the results of calculations which illustrate the general features of R_{1M} profiles for the uniaxial $S = {}^3/_2$ case, assuming a field-independent dipolar correlation time. The profiles in Figure 3 were simulated by SD, and those in Figure 4 were calculated in the constant H_S approximation. Both sets of calculations show the effect of an increasing uniaxial zfs interaction ($D = 0$, 0.05, 0.3, 1.0, and 3.0 cm^{-1}, increasing with the arrow). The water protons are assumed to

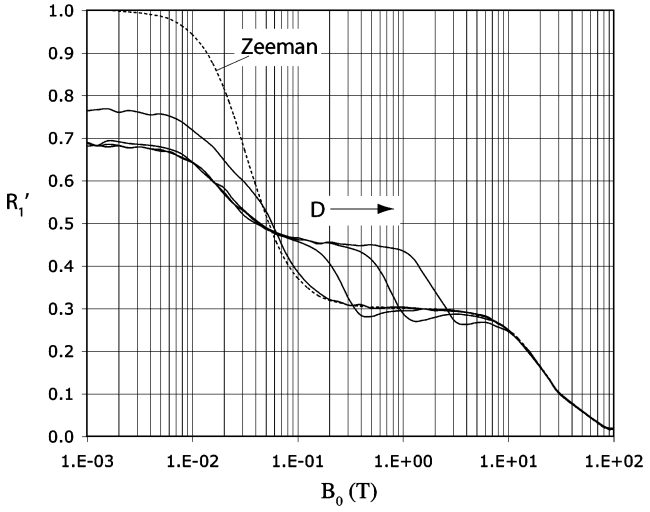

Figure 3. Theoretical MRD profiles for $S = {}^3/_2$ calculated assuming the Zeeman limit ($D = 0$, dashed line) and for $D > 0$ (solid lines) using spin dynamics simulations. The SD simulations assumed $D = 0.05$, 0.3, 1.0, and 3.0 cm^{-1} (increasing D indicated by the arrow), with other parameters listed in Table 1. R_1' is normalized to unity in the low-field Zeeman limit.

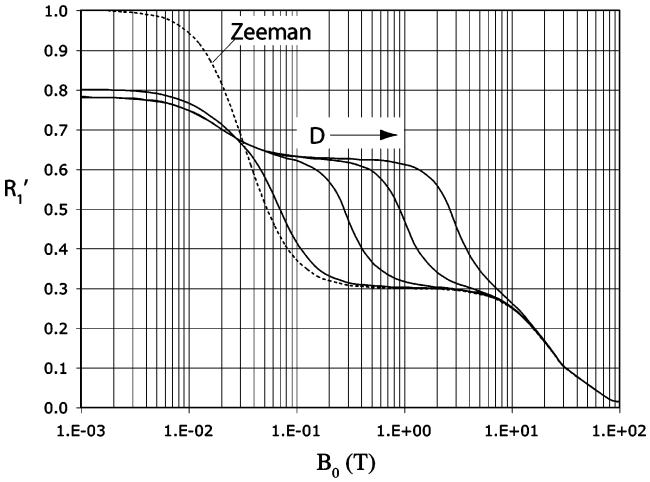

Figure 4. Theoretical MRD profiles for $S = {}^3/_2$ calculated as in Figure 2, except using the constant H_S approximation instead of SD simulations.

lie near the zfs principal axis ($\theta_{IS} = 0.28$ rad), and the dipolar correlation time is assigned a fixed value of $\tau_d = 250$ ps. These values are approximately equal to those found for Cr(III)−TSPP. It is evident that the SD profiles are qualitatively similar to the constant H_S profiles but are depressed in magnitude over much of the field range, and the dispersive features differ in their relative amplitudes. Also, the SD simulations exhibit an interesting local R_{1M} minimum on the high-field side of the midfield dispersion. This dispersive feature results from Brownian motion of the spin wave functions. It is present in the experimental profiles for Cr(III)−TSPP and Cr(III)(acac)$_3$ [13] but is absent in constant H_S profiles. It is also absent in SLE simulations,[4] which is somewhat surprising, since these methods, like SD simulation, describe the effect of reorientational diffusion on $H_S(\beta,\gamma;t)$. The difference in result probably related to the different models of reorientational diffusion employed (random walk diffusion and the classical diffusion equations, respectively, in the SD and SLE methods).

The Zeeman-limit profile (dashed), which is well-known, exhibits two well-defined dispersions, one centered at low field where $(\omega_S \pm \omega_I)\tau_{d,\perp} = 1$, the other at high field where

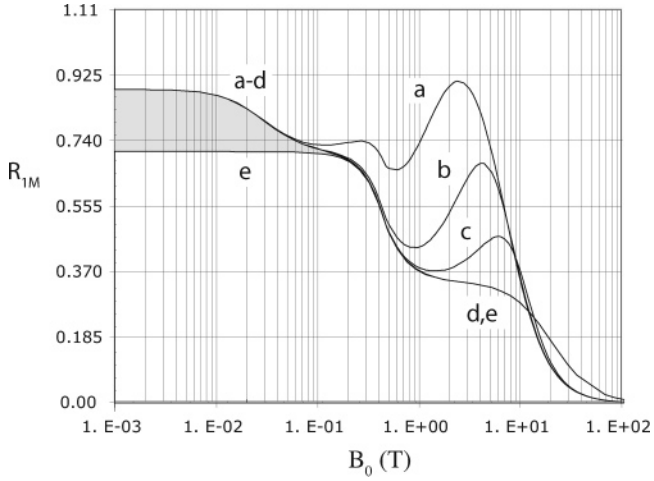

Figure 5. MRD profiles for $S = {}^3/_2$ calculated in the constant H_S approximation. The calculations assume τ_S is described by the B−M equations, with $\tau_v = 1$, 3, and 10 ps for curves a, b, and c, respectively, while curves d and e assume a field-independent value of $\tau_S = 250$ ps. The shaded region between curves d and e is the transverse contribution to R_1' due to the $|\pm{}^1/_2\rangle'$ manifold.

$\omega_I\tau_{d,z} = 1$. The high-field dispersion is often outside the experimentally accessible region. When $D \neq 0$, the profiles exhibit as many as three distinct dispersive features.[8,10,12,42]

The profiles of Figure 5 were calculated assuming that the dipolar correlation time of eq 4 is independent of magnetic field strength. If, instead, the electron spin relaxation time, τ_S, in eq 4 is described by B−M theory, the profiles exhibit a large dispersive feature in the higher-field range. Figure 5 shows constant H_S profiles calculated assuming four values of τ_v ($\tau_v = 0$, 1, 3, and 10 ps) in eq 6, with values of Δ_t^2 chosen so that τ_S approaches 250 ps in the low-field limit. Somewhat surprisingly, the experimental MRD data for Cr(III)−TSPP do not exhibit a rising dispersive feature of this kind in the high-field region, even though the Cr(III) spin system is in the vicinity of the Zeeman limit. This point is discussed further below.

The remainder of this section is a discussion, based on eq 3, of the three dispersive features that are present in the profiles calculated assuming fixed τ_S (Figures 3 and 4).

The Low-Field Dispersion. The dispersion centered at lowest field has a physical origin like that of the Zeeman-limit profile; that is, it results from Zeeman splitting of the electron spin levels. In SBM theory ($H^\circ_{zfs} = 0$, dashed curve), this dispersive feature arises from off-diagonal matrix elements of the transverse spin operators, $\langle\pm{}^3/_2|S_{x,y}|\pm{}^1/_2\rangle$ and $\langle\mp{}^1/_2|S_{x,y}|\pm{}^1/_2\rangle$, for which the eigenfrequencies are $\omega_{\mu\nu} = \omega_L$. These terms disperse away when, with rising B_0, $\omega_L\tau_{S2} \geq 1$. In the presence of a permanent zfs interaction large enough that $H^\circ_{zfs} > H_{Zeem}$, the eigenfrequency of the $\{\pm{}^1/_2 \leftrightarrow \pm{}^3/_2\}$ transition approximately equals the interdoublet splitting ($\omega_{\mu\nu} = 2\omega_D$). If it is also true that $2\omega_D\tau_{S,x}{}^{(1/2)} \geq 1$ (as occurs for Cr(III)−TSPP), the spectral density functions of these terms are negligible in eq 6a. Thus, H°_{zfs} acts to diminish the amplitude of the low-field dispersion but not eliminate it. The electron spin relaxation time controlling the low-field dispersive feature is $\tau_{S,\perp}{}^{(1/2)}$.

It should be noted that, even when $H^\circ_{zfs} > H_{Zeem}$, the electron spin motion within the $m_S = \pm{}^1/_2$ Kramers doublet has a Zeeman spatial quantization rather than a quantization along zfs principal axes; that is, $\langle S_z\rangle$, not $\langle\hat{S}_z\rangle$, is diagonal within the $m_S = \pm{}^1/_2$ manifold. Within the $m_S = \pm{}^3/_2$ Kramers manifold, the spatial quantization is along $\hat{z}$. For this reason, the Zeeman-type dispersion resulting from the $m_S = \pm{}^1/_2$ doublet persists in the

zfs limit but with diminished amplitude, since the $m_S = \pm^3/_2$ contributions are suppressed.

The Midfield Dispersion. The dispersion occurring at intermediate field strengths (called the "soft plateau" by Westlund et al.[4]) results from the change of spatial quantization of the spin motion which occurs in passing between the zfs and Zeeman limits. This feature is centered where $\omega_S \approx 2\omega_D$ ($\omega_D = 2\pi cD$), as illustrated by the calculated profiles in Figures 3 and 4. Unlike the low-frequency dispersion, the midfield feature is independent of the dipolar correlation time or of spectral density functions.

The shape of the midfield feature depends strongly on θ_{IS}, that is, on the position of the nuclear spin in the MF. The profile for a near-axial nuclear location ($\theta_{IS} = 0.28$ rad) is shown. For an equatorial nuclear position, the feature is inverted;[8,10,12] that is, R_{1p} rises with increasing B_0. The SD simulations in Figure 3 exhibit an interesting local minimum on the high-field side of the midfield dispersion that is not present for the constant H_S profiles in Figure 4. This feature was observed in the experimental profiles for Cr(III)−TSPP (see below) as well as in a previous study[13] involving Cr(III)(acac)$_3$. The R_{1p} minimum results from the effects of Brownian motion on the spin wave functions.

In terms of eq 3, all of the significant contributions to the MRD profile except for that responsible for the low-field dispersive feature arise from diagonal matrix elements, for which $\omega_{\mu\nu} = 0$. The midfield dispersive feature results from the change in spin wave functions that accompanies the changing spatial quantization that occurs in the intermediate regime. This feature arises entirely from diagonal terms in eq 3. In both the zfs and Zeeman limits, the diagonal contributions to R_{1M} vary as m_S^2, and thus, the major contribution to the MRD profile (except for the low-field dispersion) is expected to arise from the $m_S = \pm^3/_2$ levels, for which the electron spin relaxation time is $\tau_{S,\hat{z}}^{(3/2)}$ in the zfs limit and $\tau_{S,z}^{(3/2)}$ in the Zeeman limit. In the simulations, a single value, $\tau_S^{(3/2)}$, was assumed, but that assumption is strictly valid only if the transient zfs tensor has an orientation that is isotropic in the MF.

The High-Field Dispersion. The high-field dispersive feature lies outside the experimental range of field variation. In terms of eq 3, it results from the diagonal spin matrix elements ($\omega_{\mu\mu} = 0$), when the spectral density functions for those terms are suppressed at very high fields ($\omega_I\tau_{d,z} > 1$). The dispersion can also be interpreted using dipolar power plots.[31] It occurs when the nuclear Larmor frequency, ω_I, is displaced outside the dipolar power band due to $\langle S_z(0)\, S_z(t)\rangle$ at very high field strengths.

Results

UV−vis Spectra. In acid solution, the principal Cr(III)−TSPP species is the diaqua complex, which deprotonates in two steps with pK_a's of 7.63 and 11.45:[24]

$$\text{Cr(III)−TSPP}\cdot(H_2O)_2^{3-} = \text{Cr(III)−TSPP}\cdot(H_2O)(OH)^{4-} = \text{Cr(III)−TSPP}\cdot(OH)_2^{5-}$$

In the pH range 1−4, the Soret band of the porphyrin complex, shown in Figure 6A, is centered at $\lambda_{max} = 444.0 \pm 0.25$ nm.[24] At pH 7−9, shown in Figure 6B, this band shifts with rising pH to $\lambda_{max} = 436$ nm in the monohydroxo complex with an isosbestic point at 441 nm. In the pH 1−4 samples, the Soret bands observed in different buffers exhibited significant differences in line widths and extinction coefficients, although no shifts in λ_{max} occurred. We attribute these differences to effects of the medium.

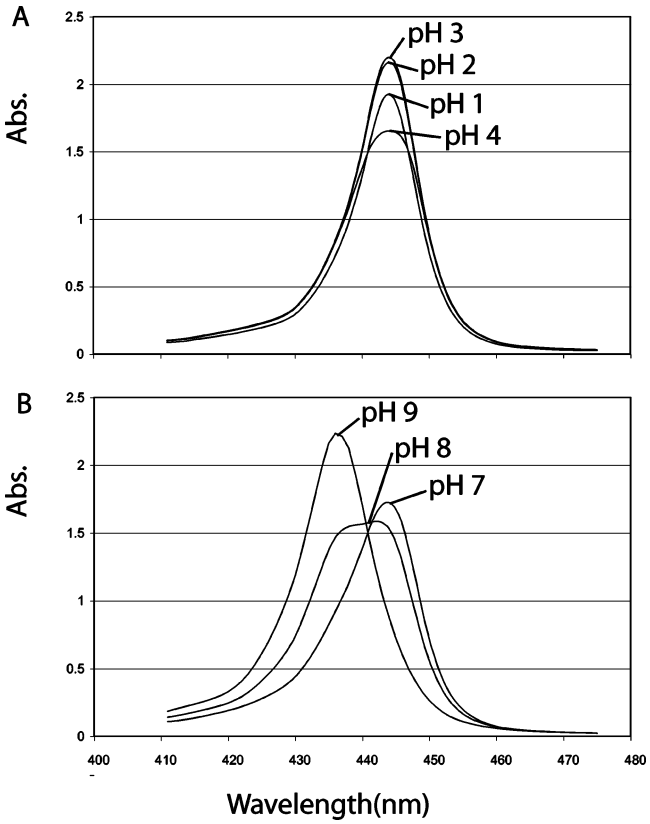

Figure 6. UV−vis spectra of Cr(III)−TSPP ($S = {}^3/_2$) in aqueous buffers of (A) (top to bottom) pH = 3, 2, 1, and 4 and (B) (right to left) pH = 7, 8, and 9. The shifts indicate the change of ligand species in the axial positions (H_2O to OH^-).

MRD Profiles. The MRD profiles for the samples prepared in acid media (pH 1−4), corrected for the diamagnetic background, are shown in Figure 7A. Those for samples in neutral to basic media (pH 7, 8, and 9) are shown in Figure 7B.

MRD Profiles at pH 1−4. The profiles in Figure 7A result from the diaqua complex. At pH 3−4, R_{1p} has a small value, which increases rapidly when the pH falls below 3, presumably due to acid-catalyzed prototropic chemical exchange. The MRD profiles at pH 3 and 4 have very small magnitudes and are nearly pH-independent, suggesting that τ_M is sufficiently long that the intramolecular R_{1p} contribution is negligible at pH 3−4. We assume that these profiles reflect the outer sphere R_{1p} contribution. The pH 4 profile was subtracted from the pH 1 profile to give the intramolecular R_{1p} contribution at pH 1, which is shown in Figure 8.

Assuming that the prototropic chemical exchange process is acid-catalyzed and assuming a simple model where $\tau_M^{-1} \propto [H^+]$, we can estimate τ_M from the pH dependence of the MRD data. Writing eq 2 at pH 1 and 2 and taking τ_M and R_{1p}, but not T_{1M} or f_m, to be pH-dependent, gives

$$T_{1M} + \tau_M^{(1)} = f_M/R_{1p}^{(1)} \qquad \text{(pH 1)} \qquad (7a)$$

$$T_{1M} + \tau_M^{(2)} = f_M/R_{1p}^{(2)} \qquad \text{(pH 2)} \qquad (7b)$$

The assumption that T_{1M} is pH-independent implies that τ_M does not contribute to τ_{dip} in eq 4, which is clearly true, since $\tau_R^{(1)}$ is

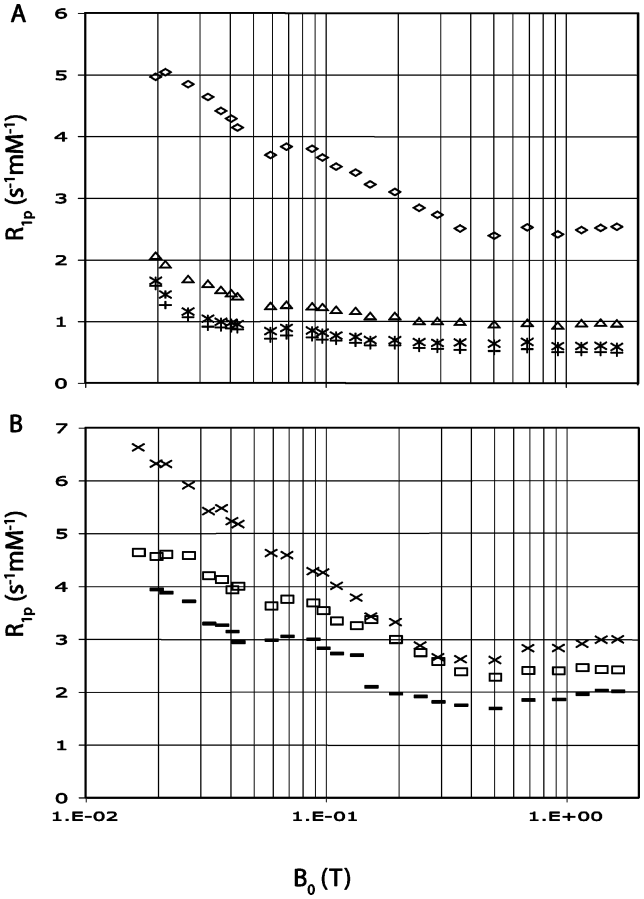

Figure 7. Experimental MRD profiles of Cr(III)−TSPP ($S = 3/2$) in aqueous buffers (20 °C): (A) (top to bottom) pH = 1, 2, 3, and 4; (B) (top to bottom) pH = 9, 8, and 7.

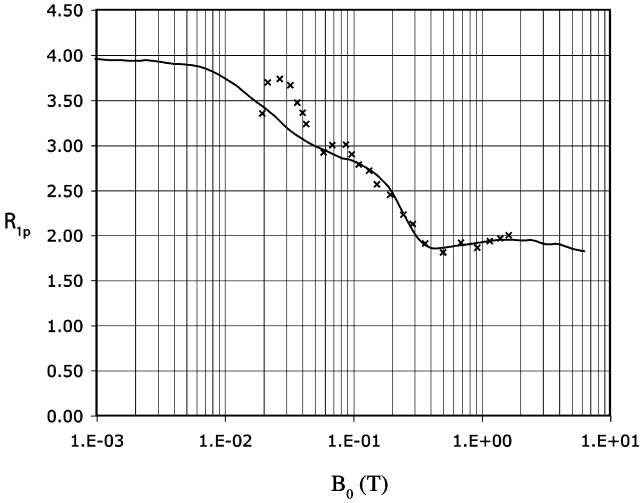

Figure 8. Spin dynamics simulations of the pH = 1 MRD profile of Cr(III)−TSPP. The physical parameters are $D = 0.27$ cm^{-1}, $\tau_M = 1.0$ μs, $\tau_S = 250$ ps, $\tau_R^{(2)} = 520$ ps, an electron-nuclear distance of 2.74 Å, and $\theta_{IS} = 0.28$ rad.

1.5 ns.[4] Subtracting eq 7a from eq 7b and assuming $\tau_M^{(2)} = 10\ \tau_M^{(1)}$ gives

$$\tau_M^{(2)} - \tau_M^{(1)} = 9\tau_M^{(2)} = f_M(1/R_{1p}^{(2)} - 1/R_{1p}^{(1)}) \qquad (7c)$$

Values of R_{1p} at pH 1 and 2 were taken from the data of Figure 7, after subtraction of the outer sphere contribution at pH 4: $R_{1p}^{(1)} = 2.5$ s^{-1} mM and $R_{1p}^{(2)} = 0.5$ s^{-1} mM at 0.2 T.

TABLE 1: Physical Parameters Used in SD Simulations of the MRD Profile[a]

varied parameters		fixed parameters	
τ_S	250 ps	θ_{IS}	0.28 rad[c]
D	0.27 cm^{-1}	E	0.0
r_{IS}	2.74 Å[b]	g_e	2.00
τ_M	1.0 μs	$\tau_R^{(2)}$	520 ps

[a] Fixed and varied parameters are shown. The value of $\tau_R^{(2)}$ is the measured value for aqueous Zn(II)−TSPP, corrected for anisotropic molecular reorientation as described in ref 4. [b] Restricted to the range 2.78 ± 0.10 Å. [c] Reference 4.

Inserting these values in eq 7 gives $\tau_M^{(1)} \approx 3$ μs for two exchangeable water protons or $\tau_M^{(1)} \approx 6$ μs for four exchangeable protons. This estimate of τ_M, of course, depends on the assumption that $\tau_M^{-1} \propto [H^+]$, which may not be quantitative in different buffers.

MRD Profiles at pH 7−9. In this pH range, the concentrations of both Cr(III)−TSPP·$(H_2O)_2^{3-}$ and Cr(III)−TSPP·(H_2O)-$(OH)^{4-}$ are significant. On the basis of the results at pH 3−4, it is clear that the diaqua complex does not contribute appreciably to the observed R_{1p} via acid-catalyzed chemical exchange. However, base-catalyzed chemical exchange is evidently rapid for at least one of the species (possibly both). The situation is more complex than that at pH 1−2, and no attempt was made to analyze the data quantitatively.

A qualitatively similar pH dependence of proton relaxivity (i.e., R_{1p} increases at both high and low pH) has been reported by Aime et al.[27] and by Woods et al.[43] in studies of Gd^{3+} complexes with tetraamide−DOTA ligands. In these complexes, chemical exchange of whole water molecules is relatively slow, and prototropic exchange is correspondingly more important in the relaxation mechanism.

Simulations of the MRD Data at pH 1. The MRD profiles at pH 1, corrected for the diamagnetic background and for the intermolecular R_{1p} contribution, were fit by SD simulation. Three parameters, D, τ_S, and τ_M, were allowed to vary without bounds, and r_{IS} was permitted to vary in the range 2.78 ± 0.10 Å. The remaining physical parameters are known fairly accurately from prior experiments and were fixed at the values given in the table. Simulations were carried out assuming both $q = 2$ and $q = 4$. The former assumption produced much better fits than the latter, which required unrealistic values of the parameters, particularly r_{IS}. This implies that the equilibrium site symmetry of Cr(III) is lower than D_{4h}. Table 1 lists the best parameters for $q = 2$. A single, magnetic-field-independent electron spin relaxation time was employed. The neglect of magnetic field dependence in τ_S is based on the absence of a rising dispersive feature at the high-field end of the MRD profile (see below).

The results of the fit are shown in Figure 8. A quantitative fit of the data over the full range of magnetic field variation was not achieved. The experimental profile is much broader than a Zeeman-only profile, clearly reflecting the influence of the permanent zfs interaction. Both the low-field and midfield dispersive features of the model calculations of Figure 3 appear to be present. It is interesting that the local minimum of R_{1p} that occurs near the high-field end of the midfield dispersive feature in the SD model calculations of Figure 3 also appears to be present in the experimental data. The properties of the midfield dispersive feature are determined principally by the absolute magnitude of D, for which the best value was 0.27 ± 0.03 cm^{-1}.

The overall profile was not well reproduced on the assumption of a single electron spin relaxation time. It appears that two

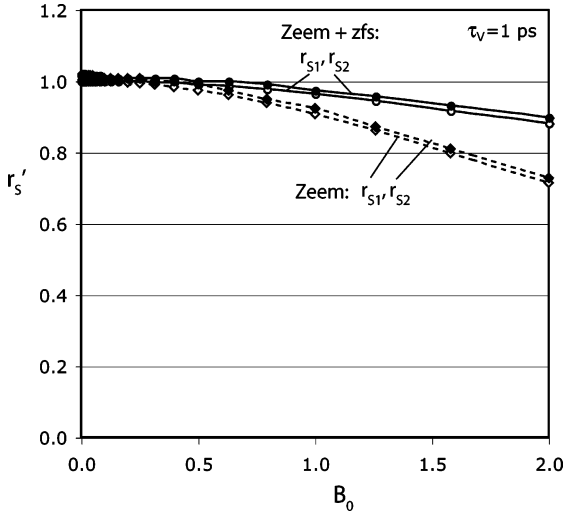

Figure 9. Magnetic field dependence of electron spin relaxation rates, r_{S1} and r_{S2}, calculated by B−M theory, eqs 5a and b (Zeem), and by eq 6a (Zeem + zfs). The calculations assumed $\theta_{IS} = 0.28$ rad and $\tau_v = 1$ ps and are normalized to unity at $B_0 = 0$.

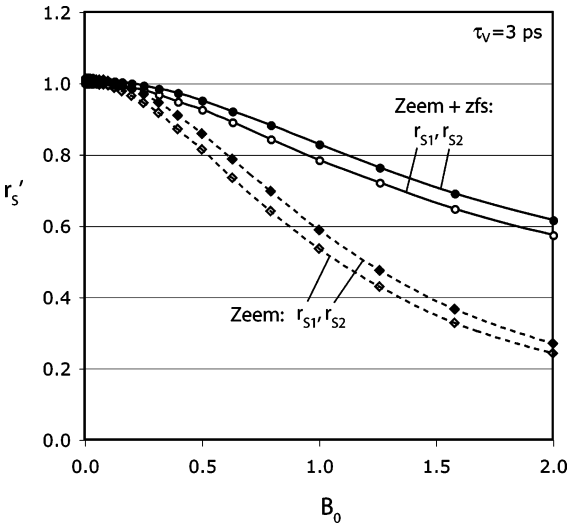

Figure 10. Magnetic field dependence of electron spin relaxation rates, r_{S1} and r_{S2}, calculated as described in the legend of Figure 9, except with $\tau_v = 3$ ps.

electron spin relaxation times, $\tau_{S,z}^{(\pm 3/2)}$ and $\tau_{S,x}^{(\pm 1/2)}$, the latter defining the properties of the low-field dispersion, are involved.

Discussion

In the data analysis, we have attempted to include all of the essential aspects of the spin physics without introducing physical parameters that are not clearly required by the data. The effects of Brownian reorientation on both H_{zfs}° and $\vec{r}_{IS}$ are obviously important. The effects of reorientation on H_{zfs}° are apparent in the lower magnitudes of the SD profiles (Figure 3) compared to the magnitudes of the corresponding profiles calculated in the constant H_S approximation (Figure 4).

We have concluded that two distinct electron spin relaxation times are needed to fit the experimental data. It is possible that electron spin relaxation may be more complex, but this assumption appears to be a minimal requirement for a satisfactory simulation. Within Parelax2, eigenstate-specific relaxation times can be incorporated in the constant H_S approximation but not in SD simulations. Thus, we do not at present have a quantitative, fully realistic way to calculate the MRD profiles of Cr(III)−TSPP.

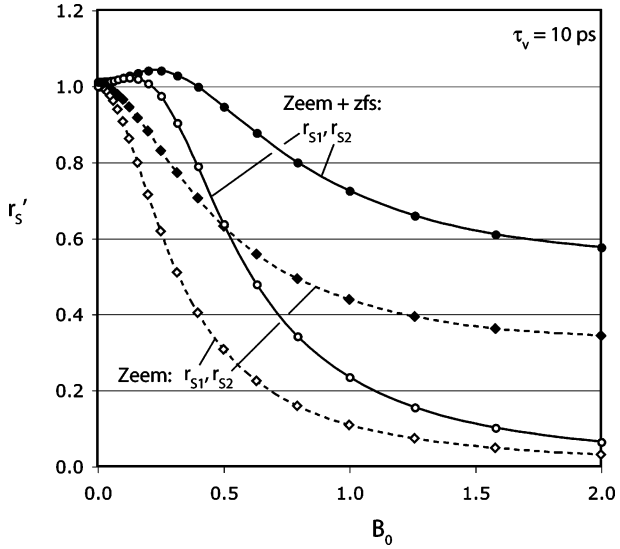

Figure 11. Magnetic field dependence of electron spin relaxation rates, r_{S1} and r_{S2}, calculated as described in the legend of Figure 9, except with $\tau_v = 10$ ps.

Magnetic Field Dependence of Electron Spin Relaxation

It was also concluded, based on the shape of the high-field end of the experimental profile, that electron spin relaxation is approximately magnetic-field-independent across the experimental range. This assumption was suggested by the very mild field dependence of the MRD data in the high-field region, where the rising dispersive feature illustrated in the model calculations of Figure 5 is not present. Similar behavior has been reported for the $S = {}^5/_2$ Mn(II)−TSPP complex, for which the D parameter is comparable in magnitude ($D = 0.2$ cm^{-1}) to that of Cr(III)−TSPP.

In B−M theory, the magnetic field dependence of τ_{S1} and τ_{S2} results from the effects of Zeeman-induced level splitting on the spectral density functions that describe collisional modulation of the zfs tensor. When a permanent zfs interaction is present, the physical mechanism is somewhat more complex. A permanent zfs tensor that is not coaxial with $\vec{B}_0$ mixes Zeeman-limit basis functions for which $\Delta m_S = \pm 1$ and ± 2. This mixing produces a band structure in the level diagram that persists even in the high-field limit. Mixing also affects the electron spin transition probabilities.

Figures 9−11 compare the magnetic field dependence in τ_{S1} and τ_{S2} predicted by B−M theory (dashed lines) and by eqs 5a and b (solid lines). Calculations are shown for three values of τ_v (1, 3, and 10 ps). The calculations using eqs 5a and b assumed $H_{zfs}^{\circ} \neq 0$ and $D = 0.27$ cm^{-1}. In B−M theory, mild field dependence in τ_S implies that τ_v is short ($\omega_S \tau_v < 1$) across the experimental range of field variation. As shown in the figures, however, the presence of a permanent zfs tensor leads to milder field dependence of τ_S at specified τ_v than does B−M theory. This difference results in part from the effect of the band structure of Figure 2 on the spectral density functions and in part from zfs-induced wave function mixing, which alters transition probabilities relative to the $H_{zfs}^{\circ} = 0$ case.

The very tight in-plane bonding of the metal ion in Me−TSPP complexes may well result in a short τ_v value. An MD simulation along the lines of that performed by Odelius et al.[44,45] to describe zfs modulation in $Ni(H2O)_6^{2+}$ would be informative in this regard. Lacking a detailed analysis of this kind, it seems likely that the observed magnetic field independence of τ_S probably results from the combined effects of a short τ_v and zfs-induced wave function mixing.

Acknowledgment. This material is based upon work supported by the National Science Foundation under Grant No. CHE-0209616.

Appendix

The Cartesian spin tensor operators, $S_q^{(2)}$, in eqs 6a and b have the following definitions:

$$S_1^{(2)} \equiv S_z{}^2 = ({}^3/_2)^{1/2}(S_z{}^2 - S(S+1)/3)$$

$$S_2^{(2)} \equiv S_{x^2-y^2} = 2^{-1/2}(S_x{}^2 - S_y{}^2)$$

$$S_3^{(2)} \equiv S_{xz} = 2^{-1/2}(S_xS_z + S_zS_x)$$

$$S_4^{(2)} \equiv S_{yz} = 2^{-1/2}(S_yS_z + S_zS_y)$$

$$S_5^{(2)} \equiv S_{xy} = 2^{-1/2}(S_xS_y + S_yS_x)$$

The numerical coefficients, $n_q^{(z)}$, in eq 6a arise from the double commutators

$$[S_r,[S_q^{(2)}, S_r]] = n_q^{(r)}S_q^{(2)} + m_{q,q'}^{(r)}S_{q'}^{(2)} \quad (r = x, y, z)$$

They have the following values:

$S_q^{(2)}$	$n_q^{(z)}$	$n_q^{(x)}$	$n_q^{(y)}$
S_{z^2}	0	3	3
$S_{x^2-y^2}$	4	1	1
S_{xz}	1	1	4
S_{yz}	1	4	1
S_{xy}	4	1	1

References and Notes

(1) Miller, J. C.; Sharp, R. R. *J. Phys. Chem. A* **2000**, *104*, 4889.

(2) Bryant, L. H.; Hodges, M. W.; Bryant, R. G. *Inorg. Chem.* **1999**, *38*, 1002.

(3) Abernathy, S.; Miller, J. C.; Lohr, L.; Sharp, R. R. *J. Chem. Phys.* **1998**, *109*, 4035.

(4) Schaefle, N.; Sharp, R. R. *J. Phys. Chem. A*, in press.

(5) Schaefle, N.; Sharp, R. R. *J. Chem. Phys.*, submitted for publication, 2004.

(6) Westlund, P.-O.; Wennerstrom, H.; Nordenskjold, L.; Kowalewski, J.; Benetis, N. *J. Magn. Reson.* **1984**, *59*, 91.

(7) Bertini, I.; Luchinat, C.; Kowalewski, J. *J. Magn. Reson.* **1985**, *62*, 235.

(8) Bertini, I.; Galas, O.; Luchinat, C.; Parigi, G. *J. Magn. Reson., Ser. A* **1995**, *113*, 151.

(9) Kruk, D.; Nilsson, T.; Kowalewski, J. *Phys. Chem. Chem. Phys.* **2001**, *3*, 4907.

(10) Nilsson, T.; Kowalewski, J. *J. Magn. Reson.* **2000**, *146*, 345.

(11) Nilsson, T.; Kowalewski, J. *Mol. Phys.* **2000**, *98*, 1617.

(12) Sharp, R. R. *J. Chem. Phys.* **1993**, *98*, 2507.

(13) Miller, J.; Schaefle, N.; Sharp, R. *Magn. Reson. Chem.* **2003**, *41*, 806.

(14) Wang, P.-L.; Lee, J.-H.; Huang, S.-M.; Hwang, L.-P. *J. Magn. Reson.* **1987**, *73*, 277.

(15) Bovet, J.-M. Ph.D. Thesis, University of Michigan, 1993.

(16) Sharp, R. R. *J. Chem. Phys.* **1972**, *57*, 5321.

(17) Abragam, A.; Bleaney, B. *Electron Paramagnetic Resonance of Transition Ions*; Dover Publishers: New York, 1986; Chapter 7.

(18) Pedersen, E.; Kallesoee, S. *Inorg. Chem.* **1975**, *14*, 85.

(19) Pedersen, E.; Toftlund, H. *Inorg. Chem.* **1974**, *13*, 1603.

(20) Singer, L. S. *J. Chem. Phys.* **1955**, *23*, 379.

(21) Luz, Z.; Meiboom, S. *J. Chem. Phys.* **1965**, *40*, 2686.

(22) Hunt, J. P.; Plane, R. A. *J. Am. Chem. Soc.* **1954**, *76*, 5960.

(23) Stranks, T. R.; Swaddle, D. W. *J. Am. Chem. Soc.* **1971**, *93*, 2783.

(24) Ashely, K. R.; Leipoldt, J. G.; Joshi, v. K. *Inorg. Chem.* **1980**, *19*, 1608.

(25) Leipoldt, J. G.; Eldik, R. V.; Kelm, H. *Inorg. Chem.* **1983**, *22*, 4146.

(26) Ashley, K. R.; Kuo, J. *Inorg. Chem.* **1988**, *27*, 3556.

(27) Aime, S.; Barge, A.; Bruce, J. I.; Botta, M.; Howard, J. A. K.; Moloney, J. M.; Parker, D.; de Sousa, A. S.; Woods, M. *J. Am. Chem. Soc.* **1999**, *121*, 5762.

(28) Solomon, I. *Phys. Rev.* **1955**, *99*, 555.

(29) Bloembergen, N. *J. Chem. Phys.* **1957**, *27*, 572; **1957**, *27*, 595.

(30) Bloembergen, N.; Morgan, L. O. *J. Chem. Phys.* **1961**, *34*, 842.

(31) Sharp, R.; Lohr, L.; Miller, J. *Prog. Nucl. Magn. Reson. Spectrosc.* **2001**, *38*, 115.

(32) Schaefle, N.; Sharp, R. *J. Magn. Reson.*, submitted for publication, 2005.

(33) Sharp, R. R. *J. Magn. Reson.* **1992**, *100*, 491.

(34) Westlund, P.-O. In *Dynamics of Solutions and Fluid Mixtures by NMR*; Delpeuch, J. J., Ed.; Wiley: 1995; p 173.

(35) Kowalewski, J.; Nordenskiold, L.; Benetis, N.; Westlund, P.-O. *Prog. NMR Spectrosc.* **1985**, *17*, 141.

(36) Abernathy, S. M.; Sharp, R. R. *J. Chem. Phys.* **1997**, *106*, 9032.

(37) Ivanov, E. N. *Zh. Eksp. Teor. Fiz.* **1963**, *45*, 1509 [English translation: *Sov. Phys. JETP* **1964**, *18*, 1041].

(38) Sharp, R. R. *J. Chem. Phys.* **1993**, *98*, 912.

(39) Sharp, R.; Lohr, L. *J. Chem. Phys.* **2001**, *115*, 5005.

(40) Westlund, P.-O. *J. Chem. Phys.* **1998**, *108*, 4945.

(41) Bertini, I.; Kowalewski, J.; Luchinat, C.; Nilsson, T.; Parigi, G. *J. Chem. Phys.* **1999**, *111*, 5795.

(42) Sharp, R. *J. Magn. Reson.* **2002**, *154*, 269.

(43) Woods, M.; Zhang, S.; Ebron, V. H.; Sherry, A. D. *Chem.—Eur. J.* **2003**, *9*, 4634.

(44) Odelius, M.; Ribbing, C.; Kowalewski, J. *J. Chem. Phys.* **1995**, *103*, 1800.

(45) Odelius, M.; Ribbing, C.; Kowalewski, J. *J. Chem. Phys.* **1996**, *104*, 3181.